

Chapter 3. High-Frequency (>100 GHz) Electronic Devices

Academic and Research Staff

Professor Qing Hu

Graduate Students

Eduard A. Garcia, Rajesh K. Gupta, Brian R. Jacobson, Zachary K. Lee, Jurgen H. Smet, Rolf A. Wyss

Undergraduate Students

Elliot E. Hui, Jason S. Kim

Technical and Support Staff

Barbara A. King

3.1 Facility for Millimeter-wave and THz Frequencies

Professor Hu's laboratory is equipped with various millimeter-wave and infrared sources which can generate coherent and incoherent radiation up to 30 THz. These include Gunn oscillators at W-band frequencies (75-110 GHz); a frequency doubler, tripler, and quadrupler using Schottky diodes at 200, 300, and 400 GHz; an optically pumped far-infrared laser which generates coherent radiation up to 8 THz; and an infrared Fourier transform spectrometer which is capable of performing linear spectroscopy from 45 GHz to 30 THz and beyond. The laboratory is also equipped with various cryogenic millimeter-wave and infrared detectors. These include Si composite bolometers, InSb hot-electron bolometers, SIS (superconductor-insulator-superconductor) receivers, and high- T_c Josephson detectors. There are many infrared cryostats which can cool the devices from 0.3 K to 77 K.

3.2 Millimeter-wave and Infrared Superconducting Focal-plane Receiver Arrays

Sponsors

MIT Lincoln Laboratory
National Aeronautics and Space Administration
Grant NAG2-693

Project Staff

Brian R. Jacobson, Eduard A. Garcia, Professor Qing Hu in collaboration with MIT Lincoln Laboratory

Although the range that includes millimeter-wave and far-infrared frequencies is one of the most

underdeveloped, these frequencies have great potential for applications in remote sensing and communication. The millimeter-wave and far-infrared frequency range falls between the two other frequency ranges in which conventional semiconductor devices are usually operated: (1) microwave frequency range and (2) near-infrared and optical frequency range.

Semiconductor devices which utilize the classical diffusive transport of electrons such as diodes and transistors have a high frequency limit. This limit is set by the time it takes for electrons to travel a certain distance. Currently, electron mobility and the smallest feature size which can be fabricated by lithography limit the frequency range to below 100 GHz. It is not likely that this limit can be pushed much higher. Semiconductor devices based on quantum mechanical interband transitions, however, are limited to frequencies higher than those corresponding to the semiconductor energy gap, which is higher than 10 THz for most bulk semiconductors. Therefore, a large gap exists from 100 GHz to 10 THz in which very few devices can operate.

The gap energies of conventional superconductors such as Nb are in the range of 100 GHz to 2 THz. This coincidence makes superconducting devices natural candidates for millimeter- and submillimeter-wave applications. At millimeter-wave frequencies, the superconducting video detectors have quantum efficiency $e/\hbar\omega$, that is, a transport of one electron for one incoming photon; while the superconducting coherent receivers have their sensitivities limited only by the zero-point fluctuation of vacuum. Such receivers have been used widely in astrophysical studies. Additional applications are feasible in space-based communication and far-infrared spectroscopy which requires the ultimate sensitivity.

We are currently developing a novel quasioptical scheme to couple the millimeter-wave and infrared signals to superconducting devices through a combination of an etched horn antenna and a planar antenna supported by a thin ($\sim 1 \mu\text{m}$) membrane, as shown in figure 1. This scheme combines the advantages of the easy fabrication of lithographic thin-film structures and the high antenna efficiencies of horn antennas. Because of the absence of substrate losses in this scheme, it is expected that a THz receiver could be constructed using all-Nb superconductor-insulator-superconductor (SIS) junctions. More important, because of the cumbersome mechanical structures used in conventional waveguide technology, microwave receivers have been single-element devices, as opposed to CCD imaging arrays at optical frequencies. Spatial scan has been achieved mechanically. Using the novel quasioptical scheme mentioned above, focal-plane detector arrays can be fabricated lithographically on a single Si wafer, as shown in figure 2, so that far-infrared imaging becomes feasible.

The first step of this project is to demonstrate the feasibility of fabricating high-quality SIS devices on free-standing SiN membranes and then to demonstrate that these devices can survive thermal cycling. Using the microfabrication facilities in Group 86 at MIT Lincoln Laboratory, we have fabricated several wafers of SIS junctions with a critical current density of $4,000 \text{ A/cm}^2$. We then etched the Si wafer underneath anisotropically in a KOH solution. A view of an SIS junction with a log-periodic antenna on a $1\text{-}\mu\text{m}$ thick SiN membrane is shown in figure 3. Extreme care was taken to protect the SIS junctions from the KOH etchant during the anisotropic etching. Figure 4 shows the I-V curves of the SIS junction measured before and after the Si wafer was etched away. There are no noticeable changes in the I-V characteristics of the device. Clearly, our work has established the feasibility of building millimeter-wave SIS receivers using micro-machined horn antenna structures.

3.3 Photon-assisted Quantum Transport in Quantum Point Contacts

Sponsor

National Science Foundation
Grant ECS 91-09330

Project Staff

Rolf A. Wyss, Professor Qing Hu, in collaboration with Christopher C. Eugster, Professor Jesús A. del Alamo

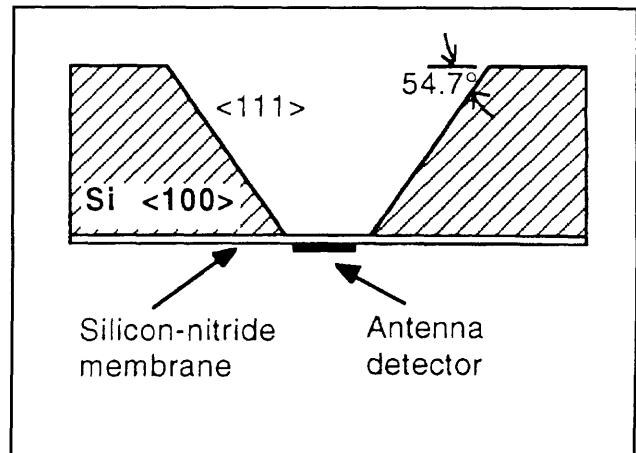


Figure 1. Example of anisotropic etching in a $\langle 100 \rangle$ silicon wafer. The opening of the wafer yields a pyramidal horn with a flare angle of 35.5° .

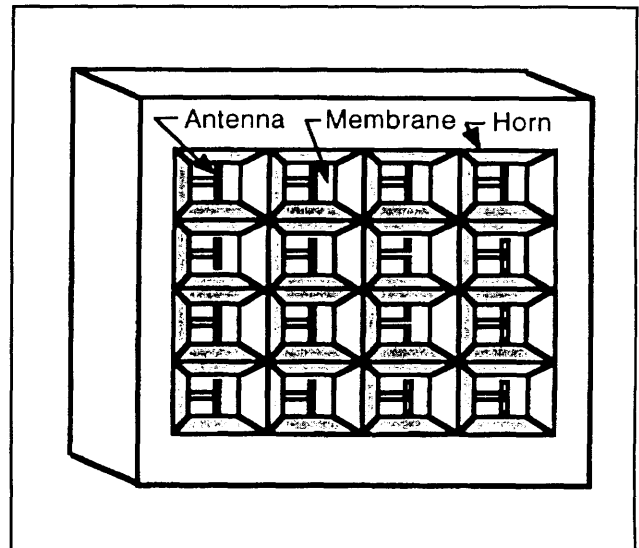


Figure 2. Perspective view of a two-dimensional horn imaging array.

Quantum transport has been one of the most active fields in solid-state physics in recent years. Advances in material preparation have made quantum phenomena profound in electron transport for many semiconductor quantum devices such as quantum point contacts, quantum dots, quantum wires, quantum wells, superlattices, etc. In clean samples and at low temperatures, electrons can travel through the whole sample without suffering phase-destructive scattering. Extensive work has been done to study various features of such phase-coherent quantum transport. However, so far the experiments reported are limited to dc transport measurements or far-infrared spectroscopy measurements.

It is well known in the field of superconducting tunneling that photons can assist the tunneling

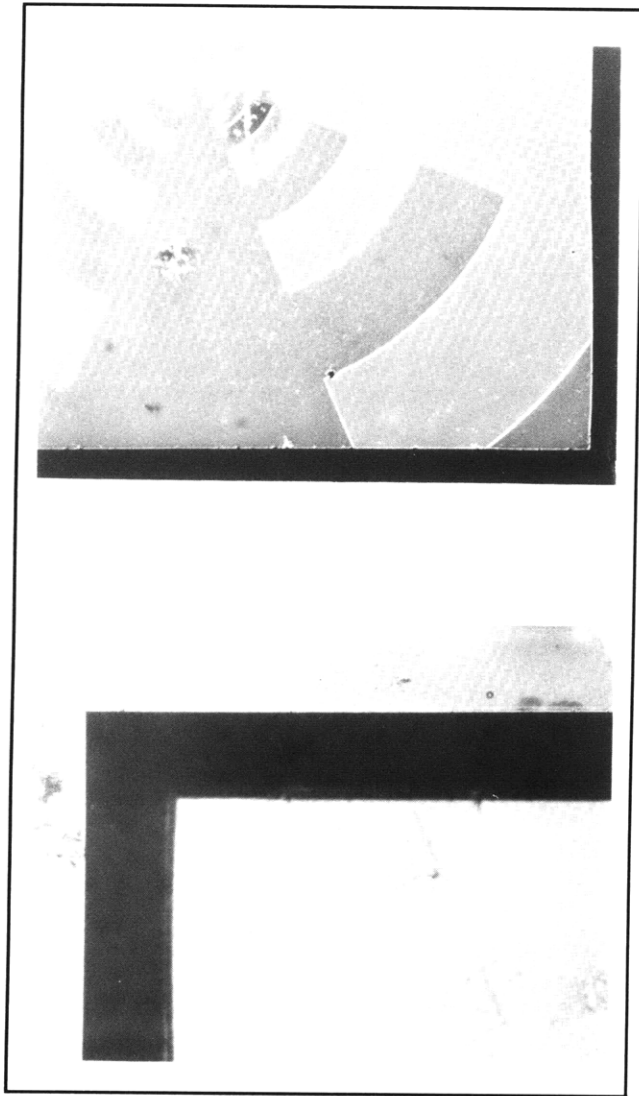


Figure 3. Perspectives on a silicon nitride membrane structure. (top) View of device seen through the membrane using backside illumination on microscope. (bottom) View of same device using top-side illumination; the 70° angle of the anisotropic etch can be made out by noticing the dark rim around the border of the device.

process, provided the tunneling is elastic so that electrons do not suffer inelastic scattering. In a broad sense, elastic tunneling is a phase-coherent quantum transport in a classically forbidden region. Therefore, all the results of photon-assisted tunneling can be applied to the study of photon-assisted quantum transport in semiconductor devices. This will provide a new dimension to study the exciting quantum transport phenomena. Novel long-wavelength optoelectronic devices may also emerge from this research.

In this NSF-sponsored project, we are studying the interaction between far-infrared photons and ballistic electrons in quantum point contact devices,

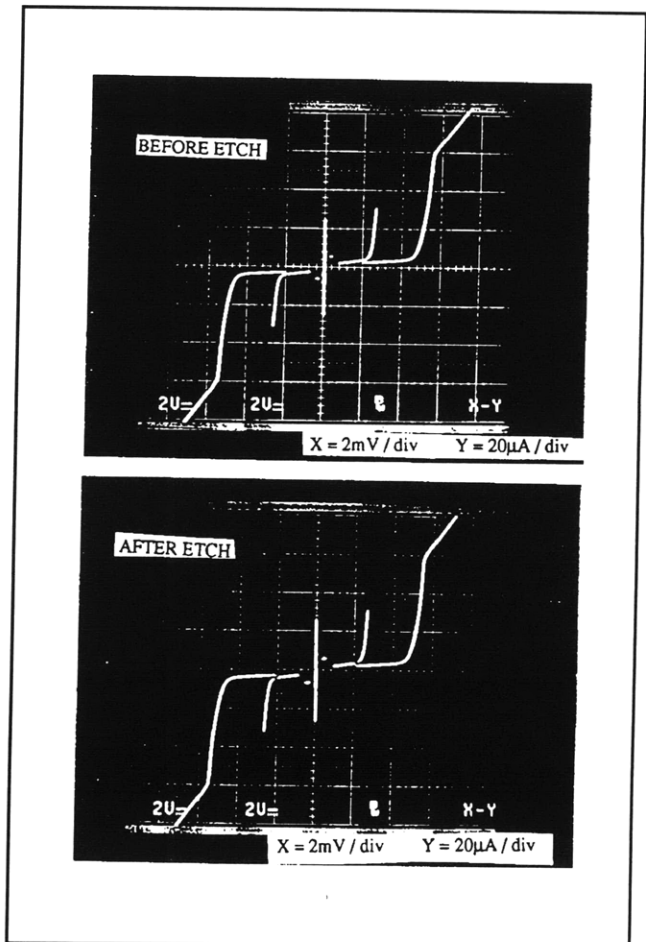


Figure 4. DC I-V curves for a device on SiN membrane (top) before etching, and (bottom) after etching the Si wafer in KOH.

whose schematic is shown in figure 5(a). We have fabricated several antenna-coupled quantum point contact devices using a combination of optical and electron-beam lithography. Figure 6 shows the SEM photographs of one of the devices. The split-gate electrodes (the vertical leads) also serve as the terminals of a log-periodic antenna, whose function is to couple the far-infrared radiation of millimeter wavelength to the point contact of submicron dimensions.

The dc transport measurement of the drain/source transport showed fifteen quantized conductance steps, indicating the high quality of the devices. Under a coherent far-infrared radiation (285 GHz), a profound photon-induced drain/source current is produced throughout a gate voltage range in which the device exhibits the behavior of a one-dimensional electron system. The amplitude of the photon-induced current is comparable to that corresponding to a quantized conductance step, and it oscillates with the gate voltage with a period corre-

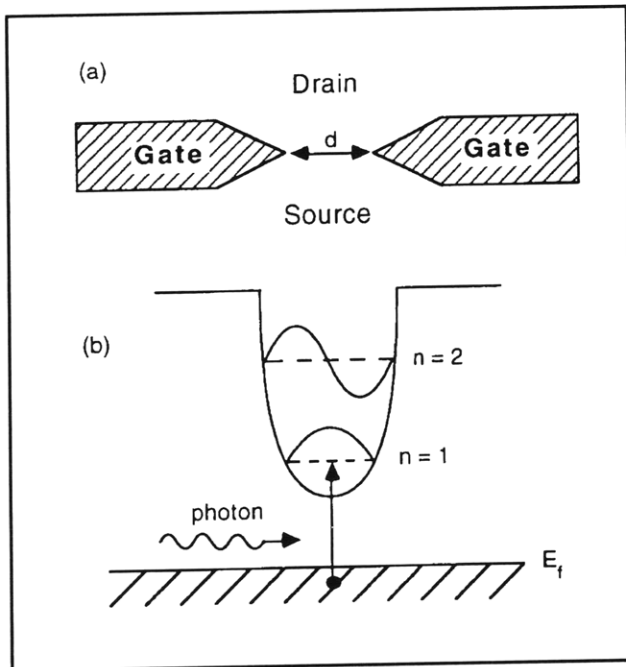


Figure 5. (a) Schematic of a quantum point contact. (b) Schematic of an electron waveguide which can be used to analyze the transport of electrons through the quantum point contact shown in (a).

sponding to the gate voltage between adjacent conductance steps, as shown in figure 7.

Our preliminary analysis suggests that the observed far-infrared photon-induced drain/source current is mainly due to heating (or a bolometric effect). Since the excitation in the two-dimensional electron gas is gapless, energy absorption can occur everywhere within the electron gas. Thus, the effect of photon-assisted quantum transport will always be accompanied by an effect due to heating. This aspect is quite different from photon-assisted tunneling in superconducting tunnel junctions in which the superconducting energy gap prevents energy absorptions in the leads. Our analysis also suggests several improvements must be made to enhance the effect of photon-assisted quantum transport and minimize the heating effect. According to the recently developed theory of photon-assisted quantum transport, the photon-assisted process mainly occurs near the classical turning points of the subbands under concern. Thus, to enhance the photon-assisted quantum process, it is crucial to concentrate the radiation field in the central region of the point contacts. This requires use of thick ($\sim 2000\text{\AA}$) antenna terminals made of good conductors. The quantum effect can also be enhanced by irradiating the devices at frequencies much higher than 300 GHz so that the photon energies are much greater than the thermal broadening of the Fermi surface.

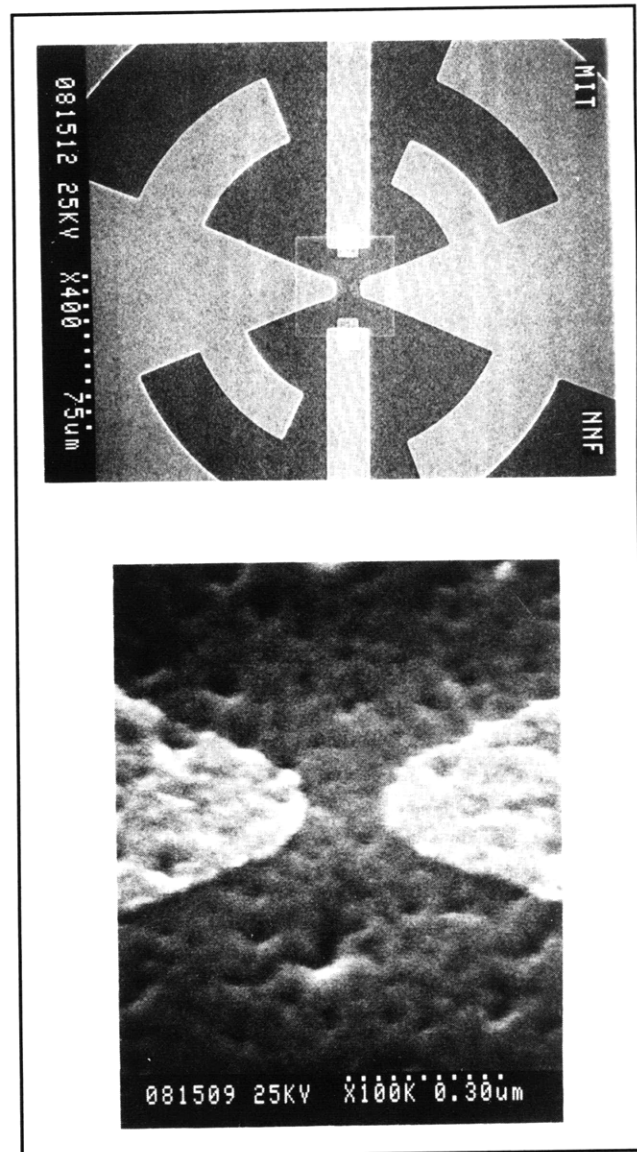


Figure 6. (a) SEM (with a magnification of 400) of a quantum point contact with log-periodic antenna. (b) Central region of the quantum point contact. The opening of the split-gate electrodes is $0.15\ \mu\text{m}$.

3.4 High- T_c Superconducting Josephson Devices

Sponsor

Defense Advanced Research Projects Agency
Contract MDA972-90-C-0021

Project Staff

Rajesh K. Gupta, Professor Qing Hu, in collaboration with Twente University, The Netherlands

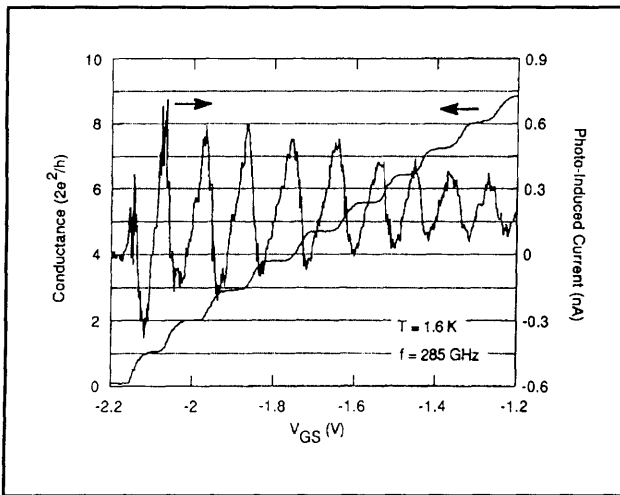


Figure 7. Drain/source conductance and the photon-induced drain/source current as functions of the gate voltage in a region where the conductance steps (measure without radiation) are well defined.

Many superconducting analog devices have been demonstrated to have higher sensitivities, higher speed and frequency limit, and lower power dissipation than competing semiconductor devices. Among them, the most successful ones are Superconducting QUantum Interference Devices (SQUIDS) and millimeter-wave detectors.

The discovery of superconductors with a superconducting transition temperature higher than liquid nitrogen temperature (high- T_c superconductors) has opened up new and exciting possibilities in electronic device technology. A high temperature version of the superconducting devices mentioned above will find a much wider range of applications wherever refrigeration is a problem. The key element of all superconducting analog and digital devices is the Josephson junction. This junction is formed by two superconductors weakly coupled together electrically. The supercurrent flowing through the Josephson junction oscillates at the Josephson frequency $f = 2eV/h$ (500 GHz/mV) when a voltage is applied across the junction. Most of the useful applications of Josephson devices result from this high-frequency oscillation. These devices include high-frequency and high-speed signal processors and high-sensitivity SQUID magnetometers whose high precision results from averaging over many cycles of the Josephson oscillations.

In collaboration with the Dutch group headed by Professor Horst Rogalla, which is the leading group in fabricating high-quality high T_c Josephson junctions, we have studied the response of a

YBCO/PBCO/YBCO ramp-type junction to coherent radiation at 176 GHz and 270 GHz. The I-V characteristic of the junction closely resembles the prediction of the resistively-shunted-junction (RSJ) model. The critical current and normal resistance product $I_c R_n$ of the junction is 0.25 mV at 5 K. The millimeter-wave radiation is coupled to the junction via a quasioptical structure that focuses the radiation onto the junction through a yttrium-stabilized ZrO_2 substrate. At 176 GHz, we have observed as many as six Shapiro steps at the maximum power level of our Gunn Oscillator-pumped frequency doubler. This implies a Josephson oscillation up to 1 THz. Shapiro steps are still visible up to 65 K, as shown in figure 8.

The amplitudes of the zeroth, first, and second Shapiro steps, as functions of the square root of the radiation power, agree remarkably well with a Bessel function fit, as shown in figure 9. This Bessel-like behavior is an indication that the junction is voltage-biased at the radiation frequency. This is in great contrast to other experiments carried at lower frequencies, where a current-biased behavior is usually observed. For a voltage-biased RSJ-like junction, the detector response can be predicted analytically. The current responsivity of our device, defined as the induced dc current per unit RF power, is calculated to be 2×10^3 A/W, which is comparable to the quantum efficiency $e/\hbar\omega \approx 1.4 \times 10^3$ A/W at this frequency.

We have also measured the response of the high- T_c Josephson junction to coherent radiation at 270 GHz. At this frequency, due to a combination of the heavy RF loss in the ZrO_2 substrate and the lack of radiation power, we have observed only the first Shapiro step.

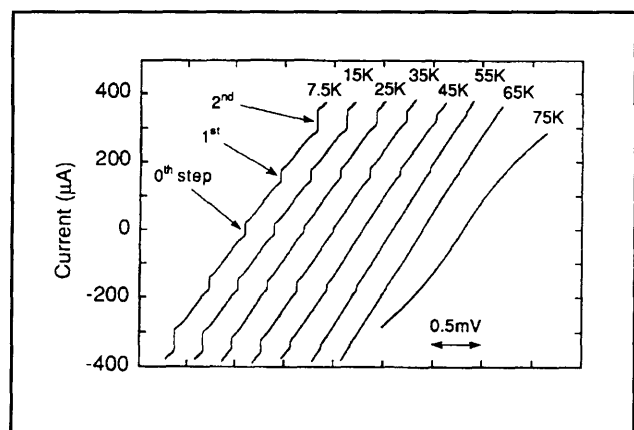


Figure 8. I-V curves of the high- T_c Josephson junction irradiated by coherent radiation at 176 GHz and taken at different temperatures. Shapiro steps are still visible at 65 K.

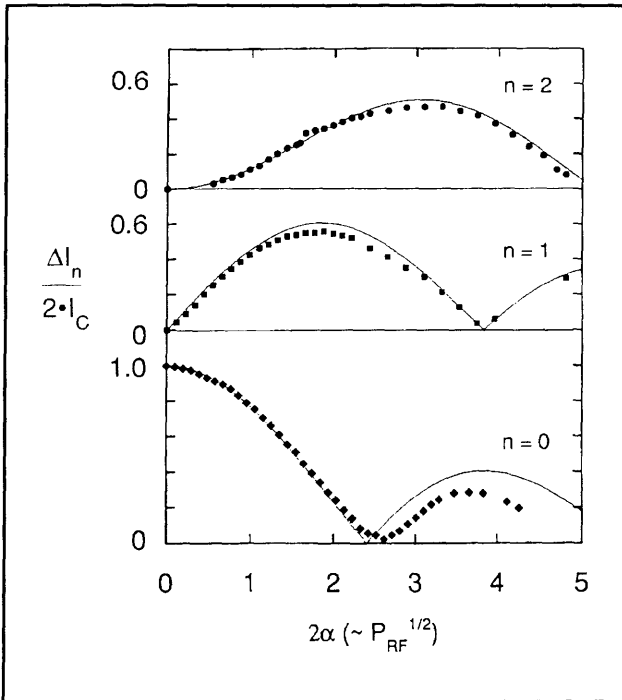


Figure 9. Measured amplitudes (normalized by the critical current in the absence radiation) of the zeroth, first, and second Shapiro steps as functions of the square root of radiation power at 176 GHz near 5 K. The solid lines are Bessel functions.

3.5 Far-infrared (THz) Lasers Using Multiple Quantum Wells

Sponsor

U.S. Army - Research Office
Grant DAAL03-92-G-0251

Project Staff

Jurgen H. Smet, Zachary K. Lee, Professor Qing Hu, in collaboration with Professor Clifton G. Fonstad, Jr.

Semiconductor quantum wells are man-made quantum mechanical systems in which the energy levels can be chosen by changing the sizes of the quantum wells. Typically, the frequency corre-

sponding to the intersubband transitions is in the far-infrared or THz range. Naturally, long-wavelength photoelectric devices, such as far-infrared lasers, which utilize the intersubband transitions have been proposed and subsequently studied.

Significant progress has been made recently toward this goal. Large oscillator strengths of intersubband transitions have been observed in far-infrared absorption spectroscopy experiments. An intersubband spontaneous emission with a power level of $\sim 10^{-7}$ W has been observed. Although these preliminary results are encouraging, two major challenges to building a quantum-well far-infrared laser still remain. One is to achieve a high degree of population inversion between two subband levels, and the other is the confinement of photons within the active region. Optical pumping suffers from low efficiency and low modulation speed. Thus, it will be difficult to achieve a sufficient gain to maintain a lasing oscillation, and, therefore, unsuitable for communication applications. As far as optical confinement is concerned, the usual dielectric waveguide confinement method, commonly used in optical and near-infrared laser systems, is not applicable at far-infrared frequencies because the confinement (on the order of a wavelength) is too large compared to the dimensions of the active region.

In this project, we will use a novel multiple quantum-well (MQW) device to circumvent these two problems. In this device, whose energy band diagram is shown in figure 10 with and without a dc bias voltage, electrons are injected selectively into an upper subband level of a wide lasing quantum well through a narrow filter quantum well. After relaxing into a lower subband in the lasing well, the electrons are then removed selectively to a collector through another narrow filter quantum well. This filter well prevents the electrons in the upper subband level from tunneling out to the collector. Using this method of selective injection and removal, a high degree of population inversion can be achieved, provided the tunneling rate of the electrons from the ground state to the collector is greater than the relaxation rate of the electrons from the upper subband to the ground state. Our calculation indicates that this should be achieved easily.

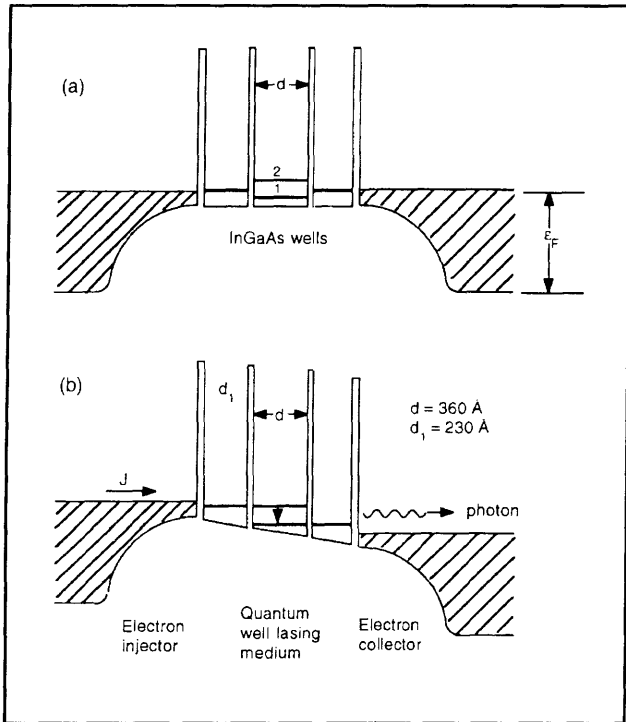


Figure 10. Band profiles (not drawn in proportion) of the proposed far-infrared laser device under (a) zero-bias, and (b) lasing condition in which $V_{\text{bias}} \sim (E_2 - E_1)/e$ $E \approx 20$ mV. The device consists of one narrow quantum-well energy filter on both sides of the lasing quantum well. The width of the narrow filter wells (made of $\text{In}_{0.53}\text{Ga}_{0.47}\text{As}$) is approximately 230 Å so the energy of its first subband lies in between the first two subbands in the wide lasing well whose width is approximately 360 Å, and will have a radiation frequency of 5 THz due to the intersubband transitions.

In the proposed MQW laser device, a parallel-plate waveguide that confines the photons can be formed between a heavily doped semiconductor injector and collector. At a doping level of $2 \times 10^{18} / \text{cm}^3$, we can raise the plasma frequency in the injector and collector to about 17 THz. It has been reported that the electron mobility, μ , for such a high doping level is $5 \times 10^3 \text{ cm}^2/\text{Vs}$. This plasma is mostly reflective with a penetration depth as short as $0.8 \mu\text{m}$ for a lasing frequency in the range of 1-8 THz. This confinement is sufficiently tight so that the lasing threshold current density is on the order of several hundred A/cm^2 , which should be achievable.

The first step of this project is to fabricate multiple-quantum-well structures with different well widths and barrier thicknesses and to perform tunneling spectroscopy on them to determine the relative positions of the subbands in different quantum wells. Because of the small energy differences which are associated with the relatively wide quantum wells, the tunneling spectroscopy must be performed at liquid helium temperatures. Our initial

measurements on the tunneling I-V characteristics revealed many features which could be attributed to elastic tunneling and LO phonon-assisted inelastic tunneling.

To interpret the fine features of the I-V characteristics with a greater certainty, we have employed a powerful method, magnetotunneling spectroscopy, to study the relative positions of the subbands. In addition to spectroscopy, this study has a practical purpose for laser applications. The nonradiative intersubband relaxation rate due to phonon emissions is much greater than that of the radiative relaxation rate. This is mainly because the transverse motion of electrons in the lasing quantum well is unrestricted, so there is a large volume in the phase space into which the electrons can be scattered. Similar to the concept employed in a tokamak to confine plasmas, a strong magnetic field will restrict the electron motions in the transverse directions. This magnetic field-induced transverse confinement, along with the longitudinal confinement provided by the quantum well, will effectively reduce the dimensionality of the electron system to that of a zero-dimensional system, exactly like that of quantum dot systems. Therefore, the nonradiative relaxation rate can be substantially reduced. Because the magnetic field does not affect the longitudinal motion of electrons, electrical pumping is still possible. This is difficult to implement for quantum dot systems which are formed geometrically.

We have performed magnetotunneling spectroscopy on a double quantum-well structure which consists of 115-Å and 200-Å $\text{In}_{0.53}\text{Ga}_{0.47}\text{As}$ quantum wells, both are confined by 30 Å of $\text{In}_{0.52}\text{Al}_{0.48}\text{As}$ respectively on the top and bottom and separated by a 60-Å $\text{In}_{0.52}\text{Al}_{0.48}\text{As}$ middle barrier. When a longitudinal magnetic field is applied, the tunneling current is modulated by the field, as shown in figure 11(a). The magnetooscillation is periodic with the inverse of the magnetic field $1/B$. Thus, a Fourier transform of this magnetooscillation in $1/B$ gives a peak which centers at a characteristic field B_0 .

The physical origin of this magnetooscillation is scattering-mediated inter-Landau level tunneling. Suppose the energy in the first well is given by $E_1 + (n_1 + 1/2)\hbar eB/m^*$, and the energy in the second well is $E_2 + (n_2 + 1/2)\hbar eB/m^*$, where E_1 and E_2 are the energies of the subbands in the first and second well under concern. In the absence of LO phonon emissions, energy conservation requires that the two energies are equal. Thus, $(n_2 - n_1)/\hbar eB/m^* = E_1 - E_2$ or $1/B = (n_2 - n_1)\hbar e/m^*(E_1 - E_2)$. This implies that whenever $1/B$ is an integer times the inverse of a characteristic field $1/B_0 = \hbar e/m^*(E_1 - E_2)$, the energy conservation is satisfied and the tunneling current will be enhanced,

which gives the oscillatory behavior of the tunneling current as a function of $1/B$, as shown in figure 11(a).

This magnetooscillation provides us with very important information about the relative positions of the subbands under concern. The energy difference between the two subbands is related to B_0 through $E_1 - E_2 = \hbar e B_0 / m^*$. Thus, the energy difference can be measured directly using the magnetotunneling spectroscopy. Since the energy difference $E_1 - E_2$ changes linearly with the bias voltage, so is the characteristic field B_0 . By measuring B_0 as a function of the bias voltage, we can determine the fraction of the total applied bias voltage dropped across the two wells.

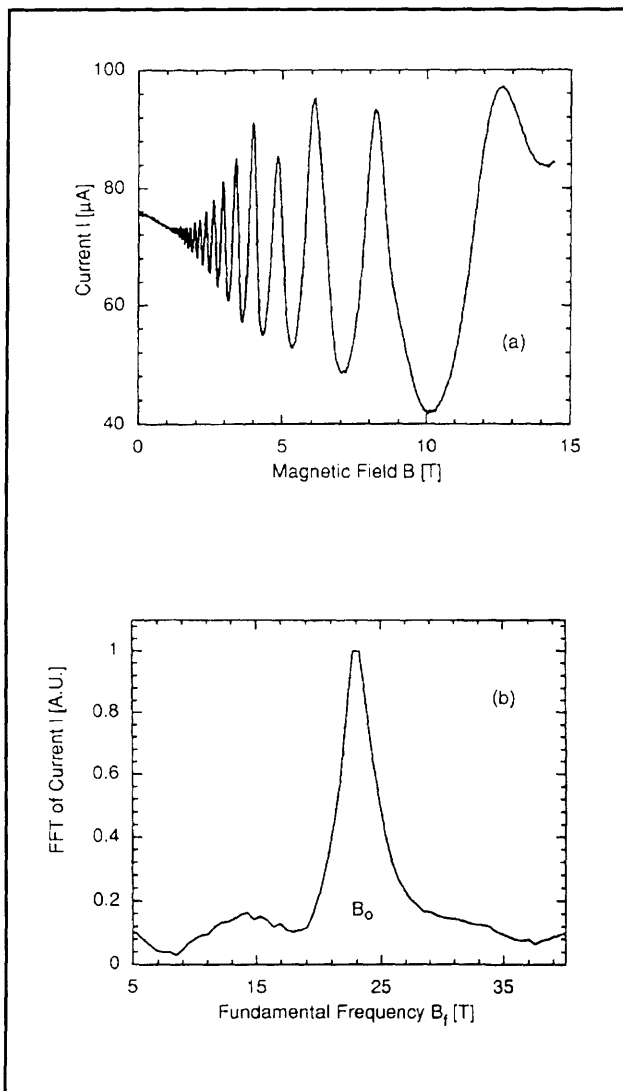


Figure 11. (a) Tunneling current (at a fixed bias voltage) as a function of the strength of a magnetic field applied in the same direction as that of the tunneling current. (b) Fourier transform of the tunneling current as a function of $1/B$.

3.6 Publications

Feng, S., and Q. Hu, "Far-infrared Photon-assisted Transport Through Quantum Point Contact Devices." Submitted to *Phys. Rev. B*, 1993.

Gupta, R., Q. Hu, D. Terpstra, G.J. Gerritsma, and H. Rogalla. "Near-millimeter-wave Response of High- T_c Ramp-type Josephson Junctions," Submitted to *Appl. Phys. Lett.*, 1993.

Hu, Q. "Photon-assisted Quantum Transport in Quantum Point Contacts." *Appl. Phys. Lett.* 62: 837 (1993).

Hu, Q., R.A. Wyss, C.C. Eugster, J.A. del Alamo, S. Feng, M.J. Rooks, and M.R. Melloch. "A Novel Submillimeter-wave Detector Using Quantum Point Contacts." *Proceedings of the Fourth International THz Conference*, University of California at Los Angeles, April 1993.

Wyss, R.A., C.C. Eugster, J.A. del Alamo, and Q. Hu. "Far-infrared Photon-induced Drain/Source Current in a Quantum Point Contact." Submitted to *Appl. Phys. Lett.*, 1993.

Thesis

Garcia, E.A. *Fabrication of All-Nb SIS Tunnel Junctions for Submillimeter-wave Detectors*. S.M. thesis. Dept. of Electr. Eng. and Comput. Sci., MIT, 1992.